UILU-ENG 86-3604

Report No. 127

MICROSTRUCTURE AND WEAR PROPERTIES OF LASER CLAD Fe-Cr-Mn-C Alloys

by

Jogender Singh and J. Mazumder
Department of Mechanical and Industrial Engineering

A Report of the

MATERIALS ENGINEERING - MECHANICAL BEHAVIOR

College of Engineering, University of Illinois at Urbana-Champaign

June 1986

MICROSTRUCTURE AND WEAR PROPERTIES OF LASER CLAD Fe-Cr-Mn-C ALLOYS

Jogender Singh and J. Mazumder
Department of Mechanical and Industrial Engineering
University of Illinois at Urbana-Champaign
Urbana, IL 61801

ABSTRACT

The laser surface cladding technique was used to form in situ Fe-Cr-Mn-C alloys on AISI 1016 steel substrate. In this process mixed powders containing Cr, Mn, and C with a ratio of 10:1:1 were delivered using a screw feed, gravity flow carrier gas aided system into the melt pool generated by a 10 kW CO_2 laser, This technique produced ultrafine microstructure in the clad alloy. The microstructure of the laser surface clad region was investigated by optical, scanning and transmission electron microscopy and x-ray micro-analysis techniques. Microstructural study showed a high degree of grain refinement and an increase in solid solubility of alloying elements which, in turn, produced a fine distribution of complex types of carbide precipitates in the ferrite matrix because of the high cooling rate. An alloy of this composition does not show any martensitic or retained austenite phase.

In the preliminary wear studies the laser clad Fe-Cr-Mn-C alloys exhibited far superior wear properties compared to stellite-6 during block-on-cylinder tests. The improved wear resistance is attributed to the fine distribution of metastable M_6C carbides.

INTRODUCTION

A great deal of attention has recently been drawn to selectively modify the mechanical properties of the metals parts (particularly wear properties) by laser cladding or surface alloying technique. Laser cladding uses a laser beam to melt and alloy powders of different composition placed on top of the substrate as well as a thin layer of the substrate. The main objective of laser cladding is to form a thin interfacial layer of an alloy on a given substrate with minimum dilution of the clad layer and to provide good surface wear and corrosion properties on the material. The advantages of this technique are many [1] but most significant advantages are: production of novel alloys, minimized clad dilution, reduced alloy material loss, reduced machining and reduced distortion, if any.

The production of surface cladding by laser technique is influenced by number of variables and interaction of these variables i.e. the power, size and shape of the laser beams, the scan velocity and the chemistry and metallurgy of the steel. For the optimum condition and for industrial application, a scheme is needed to select the best combinations for a given application. The overall composition and microstructure of the laser cladded material is also determined by the degree of mixing and cooling rate. Due to its rapid melting and quenching capabilities, usually fine microstructures, increased solid solubilities of alloying elements, non equilibrium crystalline and amorphous phases and achievement of high point defects have been reported [2-4].

The phase transformation in Fe-Cr-C ternary and Fe-Cr-Mn-C quarternary systems was studied by many investigators [2,4-6] by using different techniques such as rapid solidification process (RSP), laser alloying, and electron beam rapid quenching (EBRQ) process. They observed basic micro-

structures consisting of ferrite, martensite, fine dispersion of different carbides ($M_{23}C_6$, M_7C_3, M_6C, etc.) and some retained austenite. The formation of non-equilibrium phases, complex microstructure and complex carbides were also reported, depending upon the alloy composition [2]. They correlated different microstructures with the cooling rates (10^4 and 10^6°C/sec). The transformation product obtained in the above ternary and quarternary systems by laser cladding techniques has not been investigated. The final microstructure obtained by this technique depends mainly upon heat and mass transfer, fluid flow, and cooling rates [7].

In a recent investigation by Eiholzer, et al., it was reported that the wear properties of laser clad Fe-Cr-Mn-C alloy were found to be superior to Stellite-6 [8]. This provided great incentive for a detailed study of the transformation product in the above ternary and quarternary systems by laser techniques. The present investigation is an extension of the earlier work [9,10] and is now focused on the microstructural changes occurring in Fe-Cr-Mn-C alloy produced by laser surface cladding under different processing conditions. The optimum processing conditions were also discussed. The microstructure of the samples were characterized by optical microscopy, SEM, Auger, and STEM.

Experimental Procedure

The experimental apparatus for laser cladding consist of two units working simultaneously. Laser system, first unit, produces a beam that interacts with the substrate and powder to form the clad. The cladding treatments were carried out using a AVCO HPL 10KW continuous wave CO_2 laser with F7 case-grain optics as shown in Fig. 1. The laser was operated at a TEM^*_{01} mode*.

The beam produced by the case-grain optics was focused downward towards the substrate by a flat mirror. Cladding was done with typically 2mm beam diameter.

Powder delivery system, the second unit, delivers powder to the substrate. It consist of an Accu-Rate™ powder dispenser, funnel and argon gas inlet. The powder dispenser is a pneumatic screw feed system with a feed rate that can be varied between .017gm/sec to .19gm/sec. Powder falls from the screw into a funnel and flows to the substrate. A small amount of argon gas flows in the tube along with the powder flow. The clads produced by direct placement of powder into the molten pool, were less diluted and had less internal residual stresses. Direct placement of powder also reduces the specific energy needed for cladding, resulting in a finer microstructure [11].

Argon gas with a flow rate 7.7 gm/sec. was used to maintain a steady powder flow through the plastic tubing that leads to the substrate. It also provided the shielding of substrate which minimized surface contamination during laser processing. The plasma formation at the laser-substrate interaction point was also suppressed by the argon atmosphere. In addition, it also minimized the Mn loss and reduced the clad porosity [8].

For present investigation laser was operated at 3 and 5 KW. Cladding was performed with a defocused beam 2 mm in diameter. Specimen (6.25 mm thick) were traversed relative to laser beam at the speed of 6.35 and 8.5 mm per second. Cr, Mn, and C powders with a ratio of 10:1:1 was used for cladding on AISI 1016 steel plate, used as substrate material.

For optical microscope observation, an etching reagent consisting of 5 gm $FeCl_3$, 5 gm $CuCl_2$, 100 ml HCL and 300 ml H_2O was used. The microhardness

* Donut-shaped beam with a Gaussion Power distribution in the outer ring and none at the hole of donut.

measurements were carried out by MICROMET with a 50-gram load.

Microstructural investigations of cladded specimens were carried out by optical, Auger, and electron microprobe (EMPA) and scanning electron microscopy. After mechanical and chemical polishing to a thickness of 0.3 mm, 3 mm discs were punched from the cladded region. Specimens for TEM observations were prepared by ion-beam thinning technique and were observed using a Philips 430 microscope (attached with EDAX), operated at 300 kV.

RESULTS

1. Hardness

The hardness profile between the laser clad region and substrate is presented in Fig. 2. The top section of the laser clad region shows a high hardness value (≈ 675 VHN.) The average hardness values between the clad regions is about 550 VHN ± 50. This hardness variation is due to the presence of very fine duplex microstructure in the clad region consisted of metastable phases and carbide precipitates. The average hardness of the block precipitate is about 775 VHN (region A of Fig. 4b) and aligned phase is about 400 VHN (region B of Fig. 4b). After the laser clad/substrate interface, the hardness value dropped down to 325 VHN and then continuously decreased to 100 VHN which was the original hardness value of the substrate. The variation of hardness values from 320 to 100 VHN in the substrate is due to the heat affected zone during cladding.

2. Wear

Preliminary wear data for laser clad samples are given in Fig. 3. As a function of table speed and laser power. For comparison purpose, two additional values of both friction and wear are also presented: one was obtained from the base material of the block (AISI 1016 steel) and the other from Stellite 6. Note that for all the data presented, each data point represents the average of at least two separate tests. In addition, wear data presented in terms of "width of the wear scatter." If these data were plotted in terms of wear volume, a more dramatic difference would be between the laser clad surface and Stellite 6. The detailed experimental results of the friction and wear properties of the laser clad samples are reported elsewhere [8].

3. Microstructure

Optical microstructure of the laser clad Fe-Cr-Mn-C alloy is shown in Fig. 4(a). The microstructure consisted of unique duplex phases. The overall microstructure was divided into two parts: The part marked "A" represent white region and B represent black region. Because of very fine microstructure, optical micrograph yielded very little information. Figure 4b is the corresponding scanning electron micrograph showing the block shape phase or precipitate (Part A) and aligned structure in the matrix (Part B). These aligned structures are very fine and uniformly distributed in the matrix. However SEM micrograph did not yield any detailed microstructural information. The general survey of clad sample by EMPA shows a uniform distribution of Fe, Cr, and Mn elements in it [9]. In order to see the distribution of carbon in the clad region, Auger technique was employed and found to be uniform as shown in Fig. 5. The relative distribution of Fe, Cr, Mn and C in the clad region (as marked Part 1 and 2) is shown in Fig. 6 (a and b respectively). Auger analysis revealed that the blocky precipitates are rich in Cr, C and Fe where as remaining part of the laser clad region contained relatively less Cr and C with less amount of Fe in it. The extra peak in Auger spectra is due to etching effect (Fig. 6).

The overall structure of the laser melted zone was found to be uniform throughout. However, the clad region is again divided into two parts: the lower zone and upper zone (Fig. 4a). The width of this lower zone, which is adjacent to the clad/substrate interface, is approximately 80 μm. The composition of lower zone was found to be rich in iron (the substrate). This part of the laser clad region exhibited columnar expitaxial growth. The rest of the clad zone is consisted of about equal volume fraction of A (white) and B (black) region.

This could be explained on the basis of heat and mass-transfer model proposed by Li and Mazumder [11]. In the case of powder delivered directly at the laser beam interaction region, the total specific energy of the laser beam would be consumed by simultaneously melting the power and substrate. Because of unique fluid flow mechanism in the laser clad region, melt pool region would have homogeneous liquid solution [7,12]. The rate of cooling in laser cladding process is approximately the same as RSP process (10^5-10^6°C/sec), the melted region would rapidly solidify. During solidification, the latent heat energy would be evolved and conducted to the substrate. This latent heat energy would melt the additional layer of the substrate, and do not have enough time to remix with the remaining melt. That is why this banded zone is rich in the substrate i.e. iron phase. Away from the interface (substrate/clad) and towards the top surface of the clad region, because of high mixing, the structure is almost uniform and there is not much dilution of the laser clad alloy region. Similar findings have been observed in the other laser clad alloys such as Fe-Cr-W-C, Mg-Al and Ni based alloys [13].

Transmission electron microscopic investigation of cladded samples has been divided into two parts: A and B as shown in optical micrograph Fig. 4. In part A, fine and uniform distribution of carbide precipitates, as shown in Fig. 7, was observed in the ferrite matrix. These precipitates are generally diamond shape and their size varied from 0.1 to 0.2 μm. On the basis of diffraction pattern analysis, these precipitates have been identified as M_6C type carbide precipitate having f.c.c. structure. In high resolution microstructure of the M_6C type carbide precipitate shows some features in it. The arrows indicate that there is no continuity of the lattice planes from one end or side of the crystal to another side (Fig. 7a). In addition, after every six lattice planes, there was a faulting i.e. end-on dislocation (Fig. 7b).

This suggests that there is concentration variation within the carbide precipitate region. Because of concentration variation and high cooling rate (during liquid to solid and solid to solid state transformations) some strains could be developed in the carbide precipitate, that would lead to discontinuity of the lattice planes within the carbide precipitate crystals. The corresponding x-ray microanalysis (Fig. 8) from these precipitates are essentially rich in Cr content with partial substitution of Cr by other metals like Fe. Therefore carbide precipitates were having $(Cr, Fe)_6C$ type structure [14].

In addition to this, part "A" also contains block type precipitate as shown in Fig. 9. These precipitates are generally irregular in shape and their size varied from 0.1μm to 2.5μm. Such large differences appeared due to difference in alloy composition and cooling rates. These precipitates have been identified as Chi (χ) phase with the help of diffraction pattern and confirmed by the convergent beam techniques (Fig. 9c to e). The chi (χ) phase contained microtwins and they exhibit some crystallographic features in it (Fig. 9b). The corresponding x-ray microanalysis of the (χ) chi phase is shown in Fig. 10. The (χ) phase was found to be rich in Cr contents and also contained small amounts of Fe.

It is difficult to quantify the volume fraction of each phases present under different laser treated conditions as both of these precipitates (χ and M_6C) appeared together. However, by the general survey it was found that M_6C precipitates are finer than the χ-phase and are generally diamond shaped. In addition to that, M_6C precipitates do not contain any internal defects such as microtwins etc., whereas χ-phase always contained microtwins in it.

The crystal structure, symmetry and lattice parameters of both (χ- phase and M_6C type precipitate) phases are different, therefore these phases can be

easily differentiated by the diffraction analysis. On the other hand, it is difficult to distinguish between $M_{23}C_6$ and M_6C type carbides because of similarity in the electron diffraction pattern for these types of carbides. $M_{23}C_6$ type carbide has f.c.c. and M_6C type carbide had also f.c.c. diamond structure, and their lattice parameters are 10.621 A° and 11.08 A° respectively. With the normal heat treatment, the most common equilibrium carbide precipitate was found to be $M_{23}C_6$ type. But in the rapid solidification process many non-equilibrium phases such as χ (chi), M_6C type carbides, ε phase, martensitic phase have been reported [2]. M_6C carbides are generally observed during rapid solidification process along with the other non-equilibrium phases [15]. By the measurement of d-spacing we concluded that the f.c.c phase is M_6C phase.

A parallel TEM investigation was carried out in the part "B" of Fig. (4). The dark region was mainly consisted of elongated and very closely spaced carbide precipitates in the ferrite matrix, as shown in Fig. 11a. The average thickness of these carbide precipitates was found to vary from 0.1 to 0.4 μm and length varies up to 4 μm. The average size and volume fraction of these precipitates depend upon the laser processing conditions i.e. cooling rates. Figure 11a shows typical carbide precipitate produced at 3 kW laser power with 8.5 mm/sec traverse speed. These carbide precipitates have been identified by diffraction patterns and found to be hexagonal structure which is M_7C_3 type carbide precipitate [9,10]. The corresponding x-ray micro-analysis of M_7C_3 type carbide is presented in Fig. 11b. The M_7C_3 carbide was found to be rich in Cr content and also contained a small amount of Fe. Thus, the carbide precipitates were having $(Cr, Fe)_7C_3$ type structure [9,14]. The general survey of the TEM samples shows that the matrix is ferrite having b.c.c structures. The Cr content in the matrix is more than 40 percent (Fig. 12); thus, the posibility of martensitic transformation would be low.

DISCUSSION

The general microstructural survey of the laser clad region represented fine uniform distribution of chi (χ) phase and M_6C type precipitate and was surrounded by the M_7C_3 type carbide precipitate in the ferrite matrix. On the basis of microstructural analysis, and as reported earlier by Singh and Mazumder [9], the possible phase transformation sequence could be further modified and presented as follows:

$$L \rightarrow \alpha + L \rightarrow (\alpha + M_6C + \chi)_I + L \rightarrow (\alpha + M_6C + \chi)_I + (\alpha + M_7C_3)_{II}$$

It appeared from the above sequence that the first transformation products (I) were carbide precipitates (M_6C) and Chi phase in the α- matrix, and then equilibrium M_7C_3 carbide was formed (II). Both the M_6C carbide precipitate and Chi (χ) phases are the non-equilibrium phases. The formation of non-equilibrium phases and Chi (χ) phases has been reported in numerous alloy systems such as Fe-X-C (where X = Cr, Mo, or W), Ag-Ge, Au-Ge and Ag-Si, etc. These non-equilibrium phases are roughly classified into three kinds: namely, (1) the electron compound of Hume-Rothery type, (2) transformation products produced by short range diffusion and (3) transformation products produced by shear mechanism without short range diffusion. Judging from the fact that lattice parameter and crystal structure of χ (Chi) phase are the same as equilibrium χ phase with A12 - α Mn structure in the Fe-Cr-Mo system [12]. The present non-equilibrium Chi (χ) phase appears to be a solid solution of Cr-Fe alloys containing a super saturated amount of carbon in it. According to Inoue et al [2] the main constituent present in Chi (χ) phase is Fe. This is in contrast with the present result. The present analysis of χ-phase shows that the main constituent is Cr with relatively less

content in the ternary Fe-Cr-C system. From this it is possible to argue that the existence or formation of any austenite phase in Fe-Cr-C and Fe-Cr-C-Mn system depends not only on the composition of the alloys but also depends upon the cooling rates.

It has been observed that there was extended solid solubility of Cr in iron matrix, as shown in Fig. 13. It indicates that at low laser power (3 kw) with increasing table speed, the solid solubility of Cr increased from ~36 wt% to 49wt% in the matrix. This suggests that by controlling the laser processing conditions, the solid solubility of the alloying elements (such as Cr) can also be controlled in the matrix (iron). Similar findings have also been observed in Ni base alloys [13].

SUMMARY

A laser clad Fe-Cr-Mn-C alloy produced very fine grained microstructure of ferrite and complex carbide precipitation. The increase in solid solubility and high cooling rate produced Chi (χ) phase and M_6C type carbide precipitate first in the ferrite matrix followed by formation of an aligned M_7C_3 type carbide precipitate in the ferrite matrix. As matrix contained high Cr content (Cr $\geq$ 50%) which stabilizes ferrite, the formation of austenite or martensite was not observed. The χ-phase and M_6C type carbide precipitates were uniformly distributed in ferrite matrix with a high Cr, Mn and C concentration. The excess amount of Cr, Mn and C rejected from the first solidified phase (ferrite + χ-phase and M_6C carbide precipitation) to remaining melt gave rise to an aligned M_7C_3 type carbide precipitate in the ferrite matrix. Low laser beam power with high traverse speed (i.e. high cooling rate) would give rise to fine, uniform distribution and large volume fraction of χ-phase and M_6C carbide precipitates in the ferrite matrix. The blocky presipitates (M_6C

precipitates and x-phase) have higher hardness than the aligned M_7C_3 type carbide precipitates, therefore, they are responsible to give rise to better wear and friction properties.

ACKNOWLEDGEMENT

This work was made possible by a grant from Quantum Laser Corporation, Long Island, New York, and the University of Illinois Materials Processing Consortium. Thanks are also due to Professor C. M. Wayman for helpful discussions. The studies involving electron microscopy were performed in the Center for Microanalysis of Materials in the Materials Research Laboratory of the University of Illinois at Urbana-Champaign.

REFERENCES

1. Bill, R., Appleton, Bruce Sartwell, Paul, S. Peerey, Robert Schaefer, and Richard Osgood, Materials Science and Engineering, Vol. 20 (1985), p. 23.

2. Inoue, A., T. Iwadochi, T. Minemura, and T. Masumato, Trans. J.I.M., 22 (1981), p. 197.

3. Mawella, K. J. A., and R. W. K. Honeycombe, J. of Materials Science, 19 (1984), p. 3760.

4. Messler, R. W., G. S. Ansell, and V. I. Lizunov, Trans. ASME, 62 (1981), p. 213.

5. Molian, P. A., P. J. Wang, K. H. Khan, and W. E. Wood, in the Material Research Society Proceedings of "Rapidly Solidified Amorphous and Crystalline Alloys," ed. B. H. Kear, B. C. Giessen, M. Cohen, North Holland Publishing Company, 8 (1981), p. 511.

6. Rayment, J. J., and G. Thomas, ibid, p. 547.

7. Chande, T., and Mazumder, J., J. of Appl. Phys., Vol. 1, July 1982.

8. Eiholzer, E., C. Cusano, and J. Mazumder, Proceedings of the Intrnational Congress on Applications of Lasers and Electro-Optics," Boston, Mass., ed., J. Mazumder, published by Laser Institute of America, Vol. 44, Nov. 1984, p. 159.

9. Singh, J. and J. Mazumder, J. of Materials Science and Technology, (in press).

10. Singh, J., and J. Mazumder, "Proceedings of the International Congress on Application of Lasers and Electron Optics," San Francisco, California, published by Laser Institute of America (in press).

11. Li, L. J., and J. Mazumder, Laser Processing of Materials, AIME, (1984), p. 35, K. Murkherjee, and J. Mazumder, (Ed.).

12. Weerasinghes, V. M., and W. M. Steen, "Transport Phenomena in Materials Processing, ASME ,Vol. 10, (1983) p. 15, M. M. Chen, J. Mazumder, and C. L. Tucker, (Ed.).

13. Singh, J., and J. Mazumder, unpublished research work.

14. Interpretation Of Electron Diffraction Patterns, written by Andrews, K. W., D. J. Dyson, and S. R. Keown, Plenum Press, New York (1967), p. 197.

15. J. J. Rayment, and B. Cantor, Met. Trans., Vol. 12A, (1981), p.1557.

16. Lemkey, F. D., E. R. Thompson, J. C. Schuster, "The Quaternary System Fe-Cr-Mn-C and Aligned Ferrous Super Alloys," In-Situ Composites IV, eds., F. D. Lemkey, H. E. Cline, M. McLean, Elsivier Science Publishing Co., Inc., 1982, p. 31.

17. Thompson, E. R., and F. D. Lemkey, U. S. Patent 3,671,223, June 20, 1972.

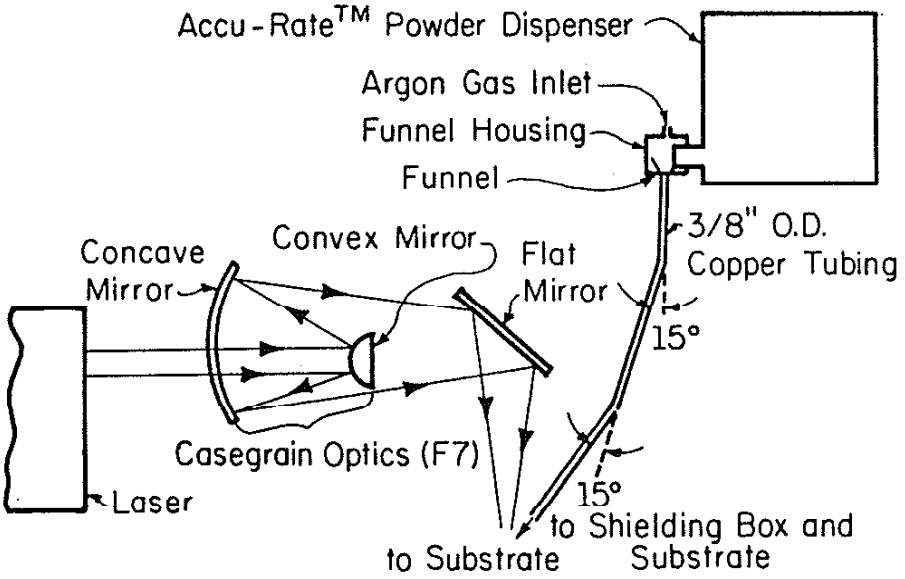

Figure 1 Optics used for Laser Cladding

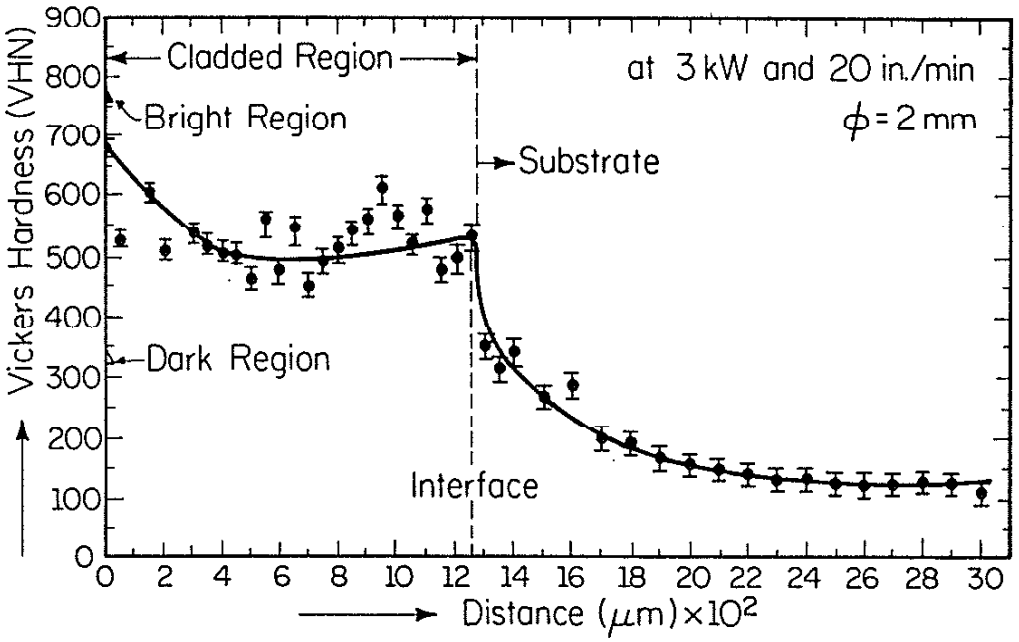

Figure 2 Hardness variation in the laser clad region.

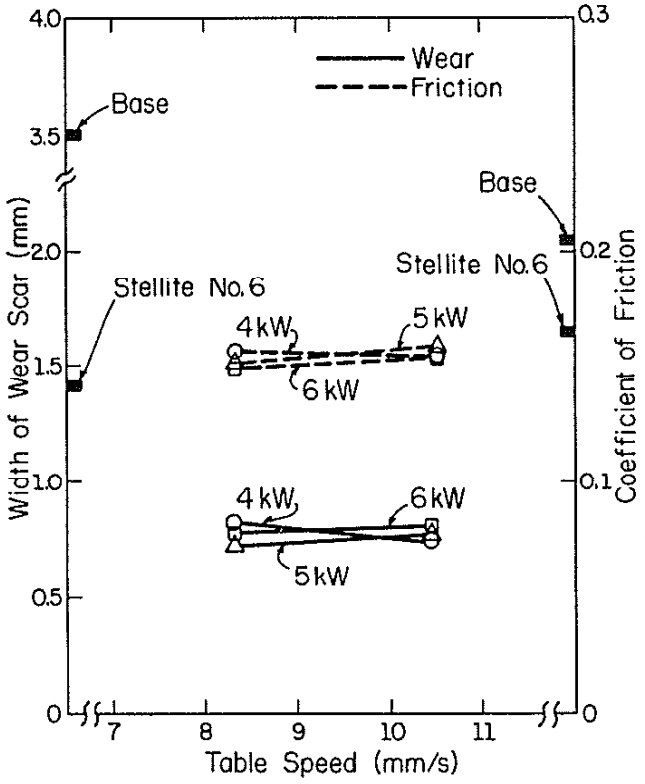

Figure 3 Friction and wear of laser clad surface as function of table speed and laser power [8].

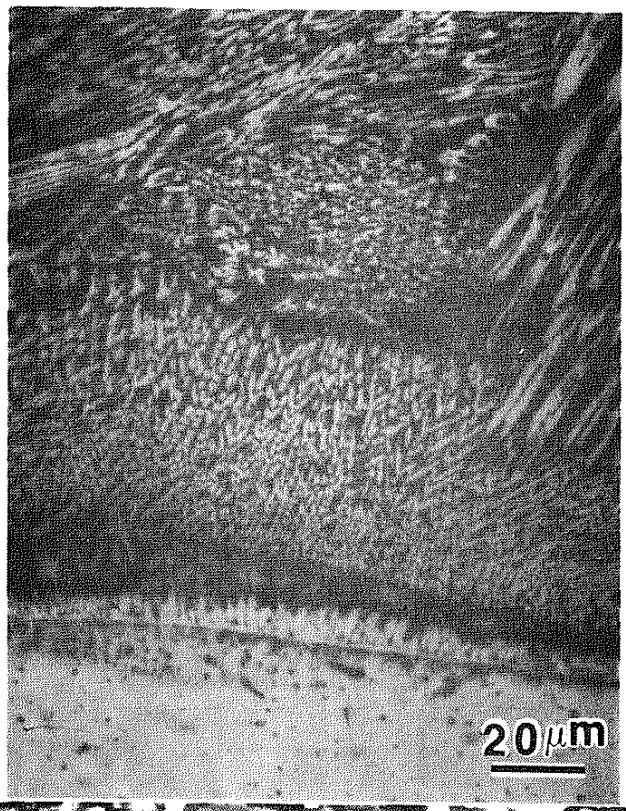

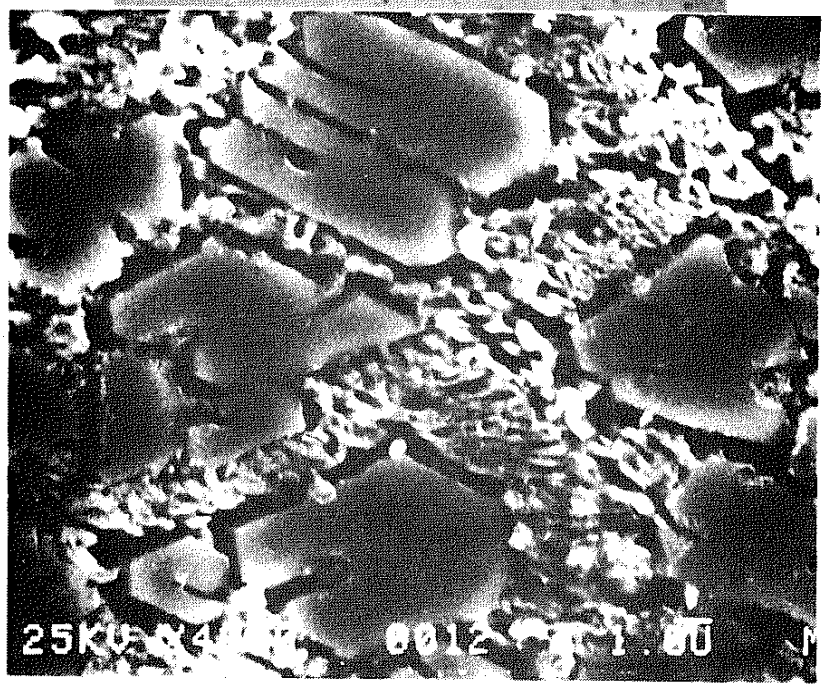

Figure 4a Optical micrograph of the laser cladded region showing duplex microstructure

Figure 4b Scanning electron micrograph of the laser clad region showing blocked precipitates (A) and elongated precipitates (B) as marked

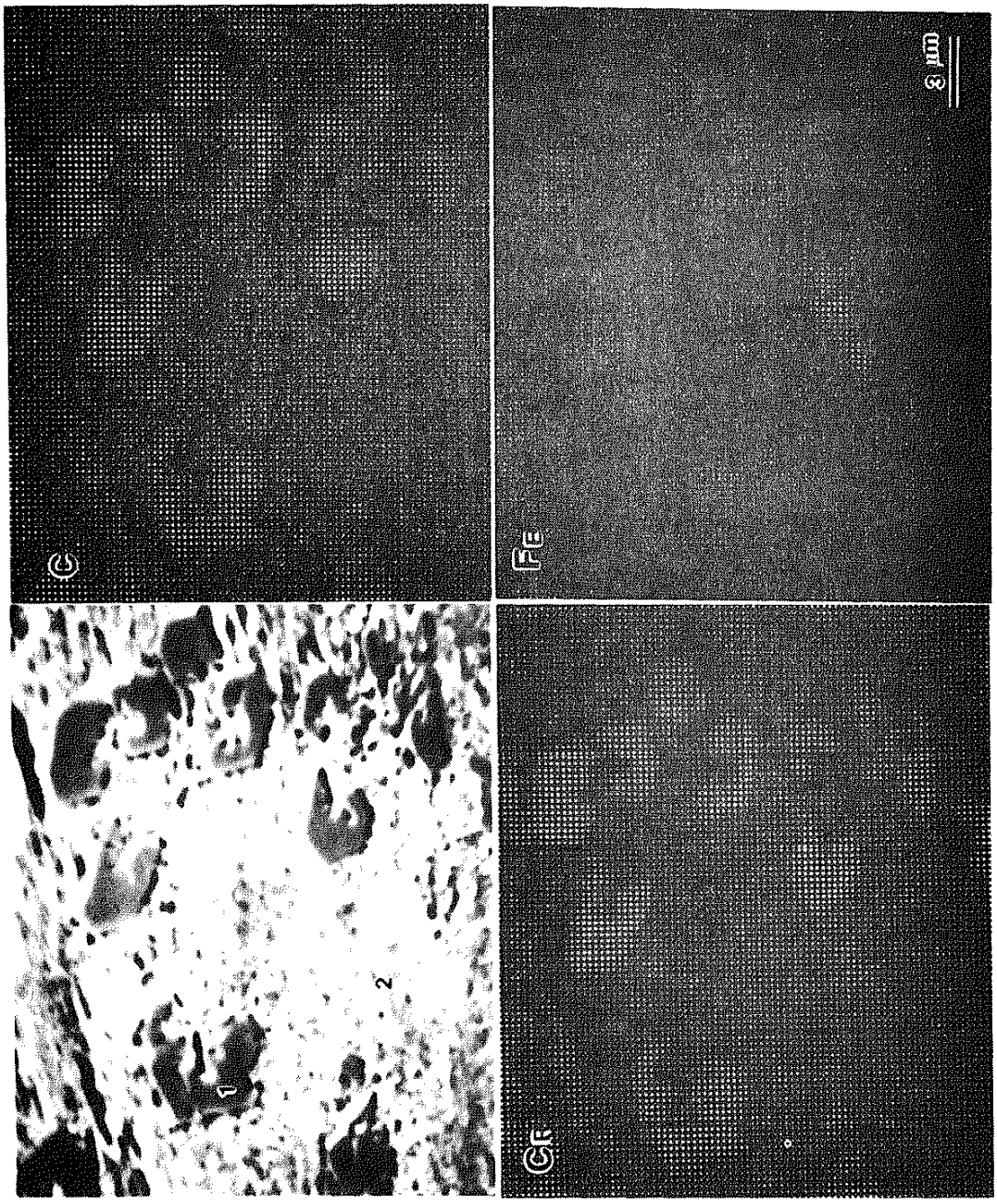

Figure 5 Dot map taken by Auger showing the distribution of Cr, C and Fe in the laser clad region

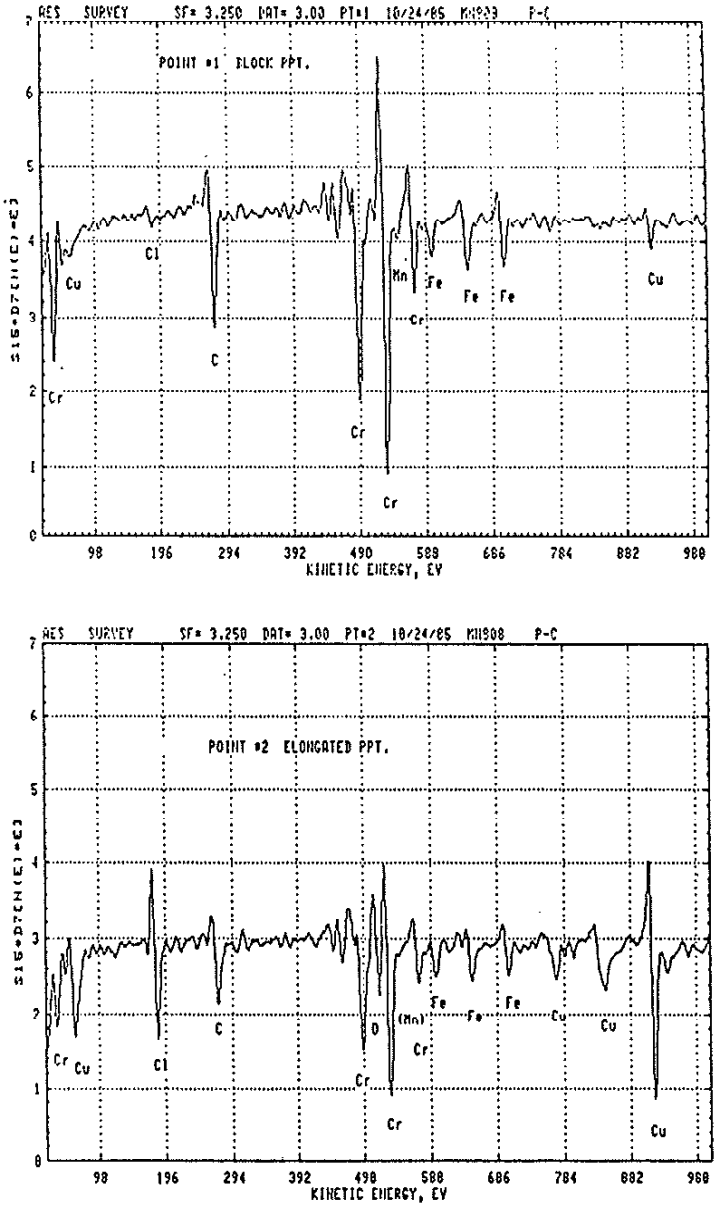

Figure 6 Scanning Auger Microprobe of the cladded region showing the relative distribution of Fe, Cr, Mn, and C segments

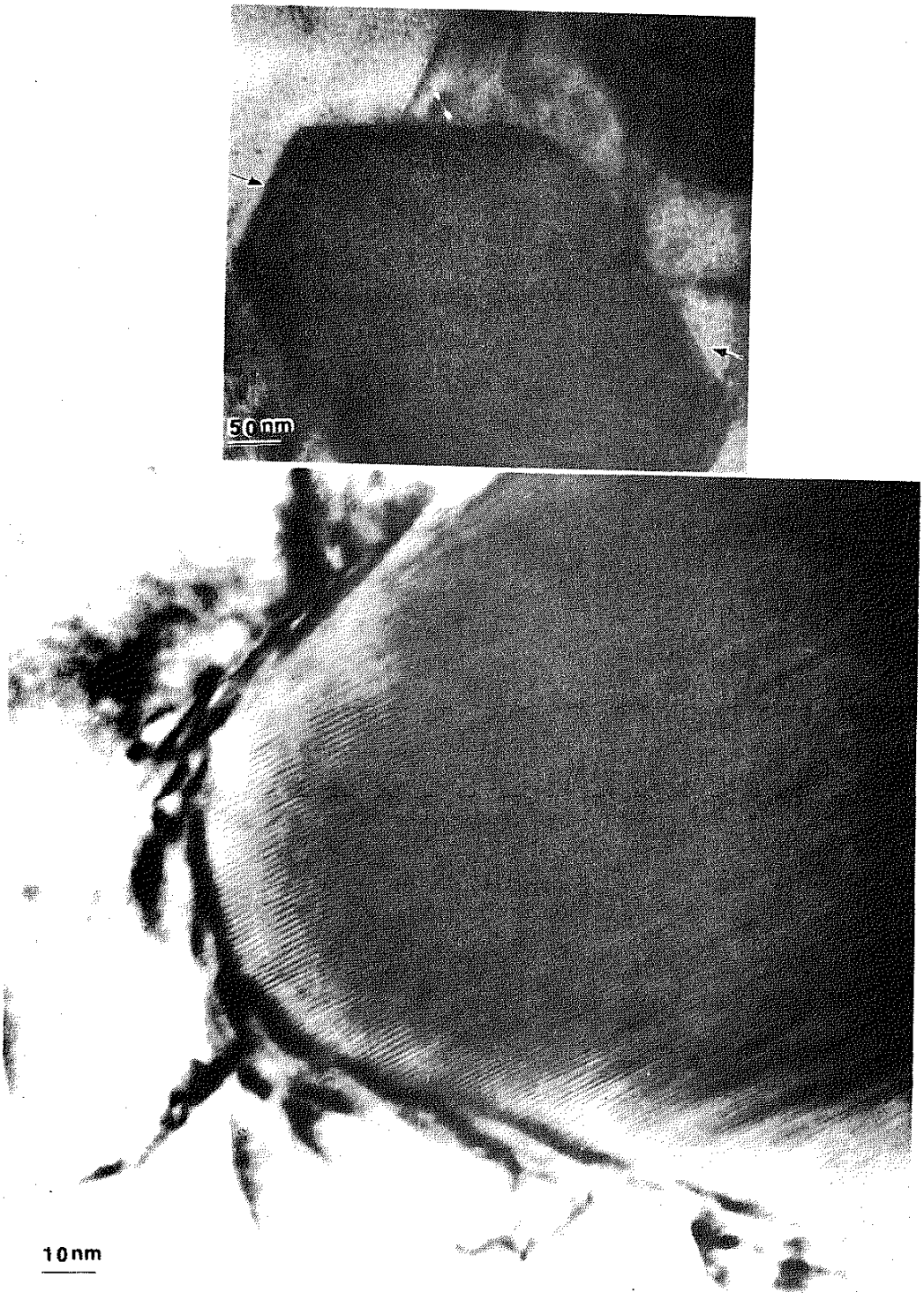

Figure 7 High resolution transmission electron micrographs (a and b) of the laser clad region showing the M_6C Type Carbide Precipitate.

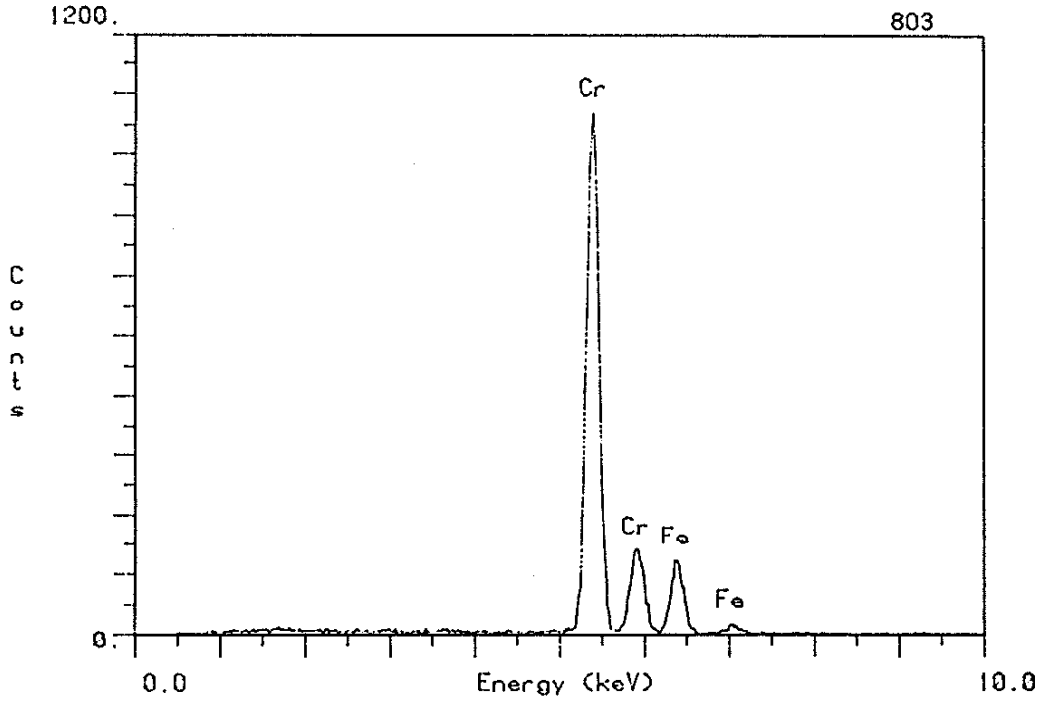

Figure 8 The STEM X-ray micro chemical analysis of the M_6C Type carbide precipitate showing that precipitate is rich in Cr Contents

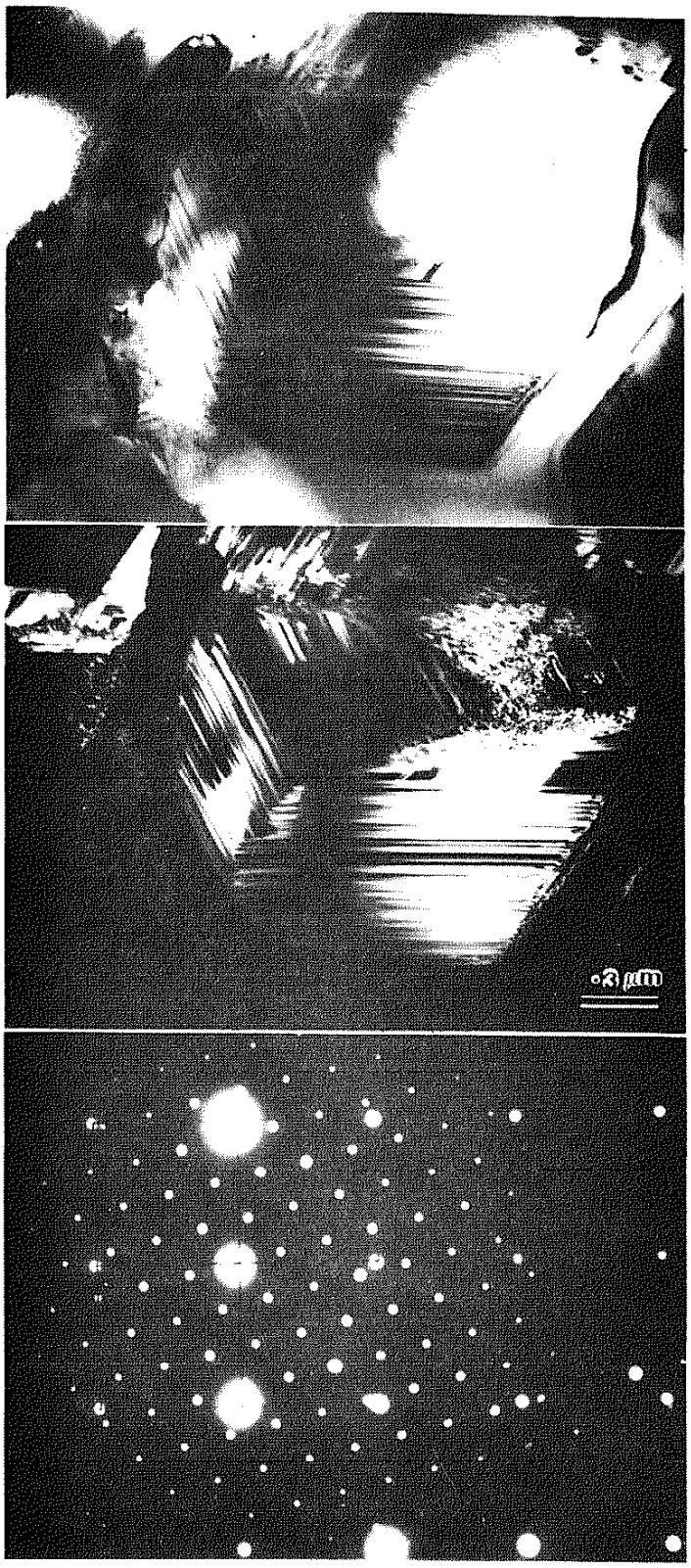

Figure 9 Transmission electron micrograph of the laser clad region showing the Chi (X) Phase is having microtwins (a) bright field, (b) dark field (c) corresponding diffraction Pattern [110] orientation; (d) and (e) are the convergent beam diffraction pattern taken at different camera length [101]. The M's refer to mirror lines

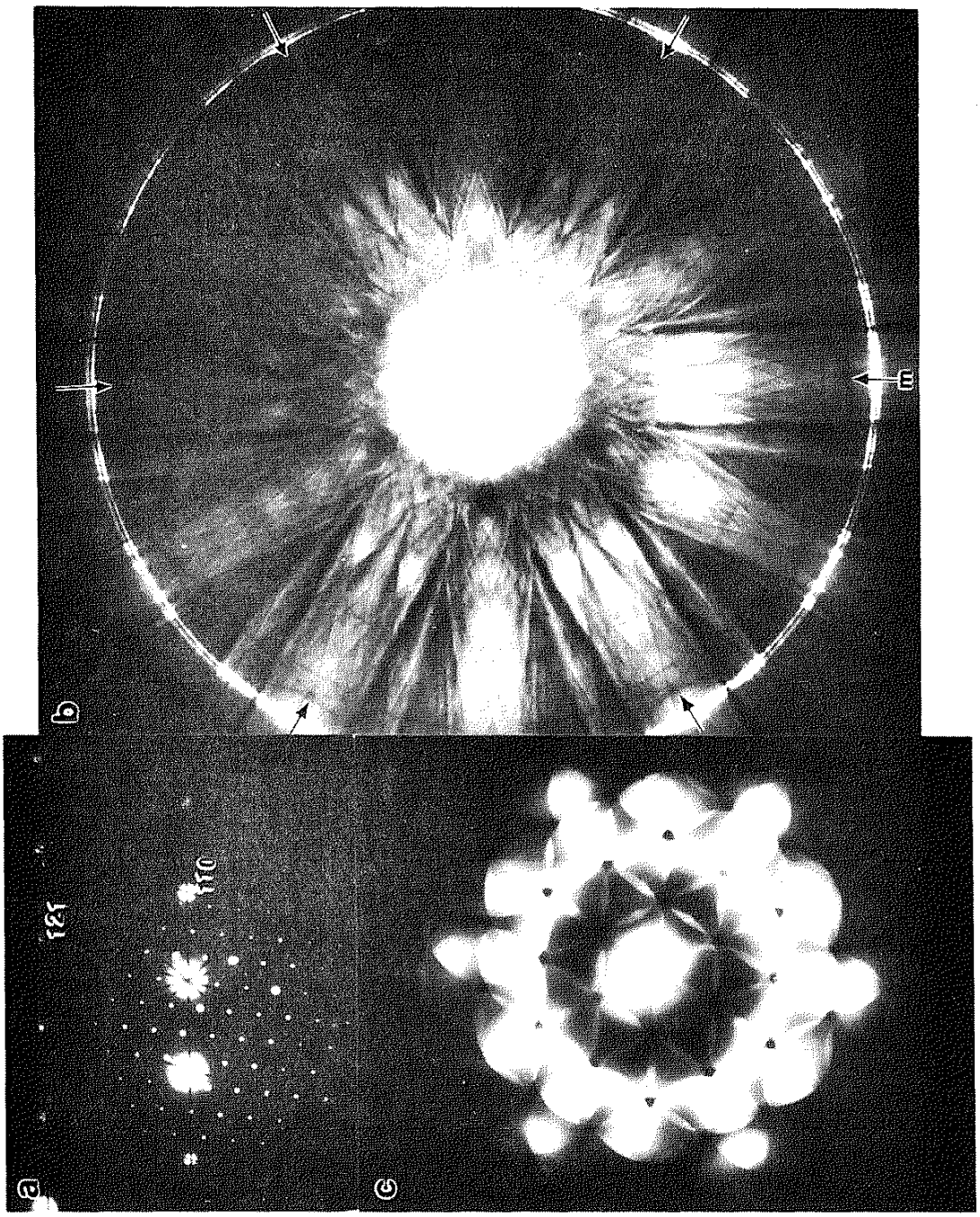
E
b
c
a
131
110

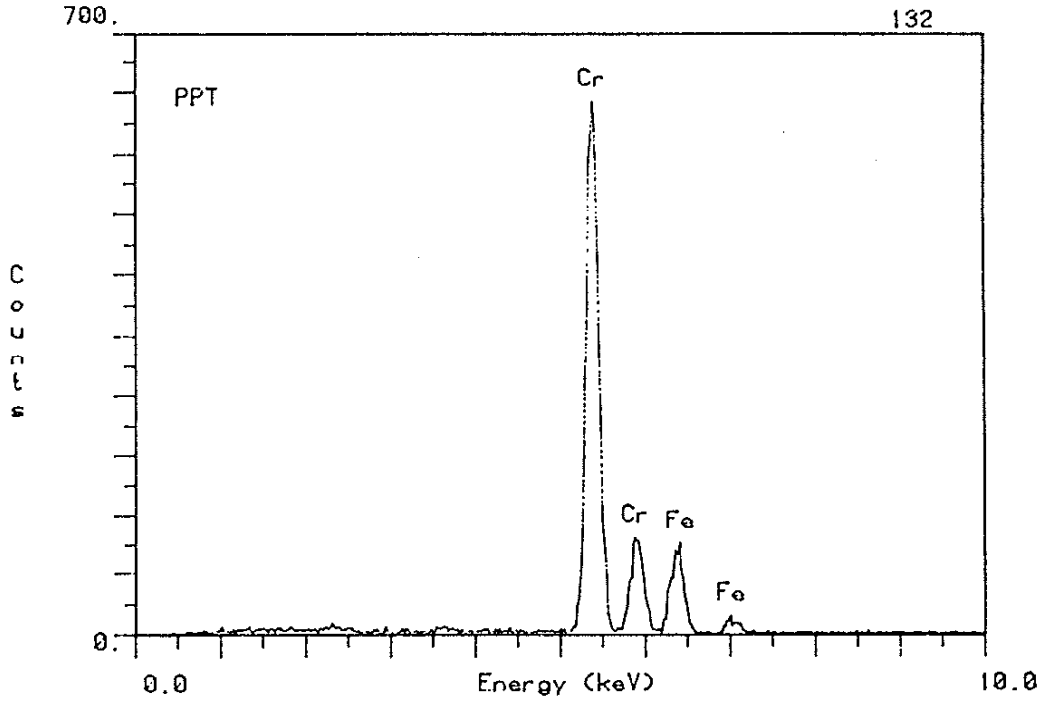

Figure 10 The STEM X-ray micro chemical analysis of the Chi (χ) Phase

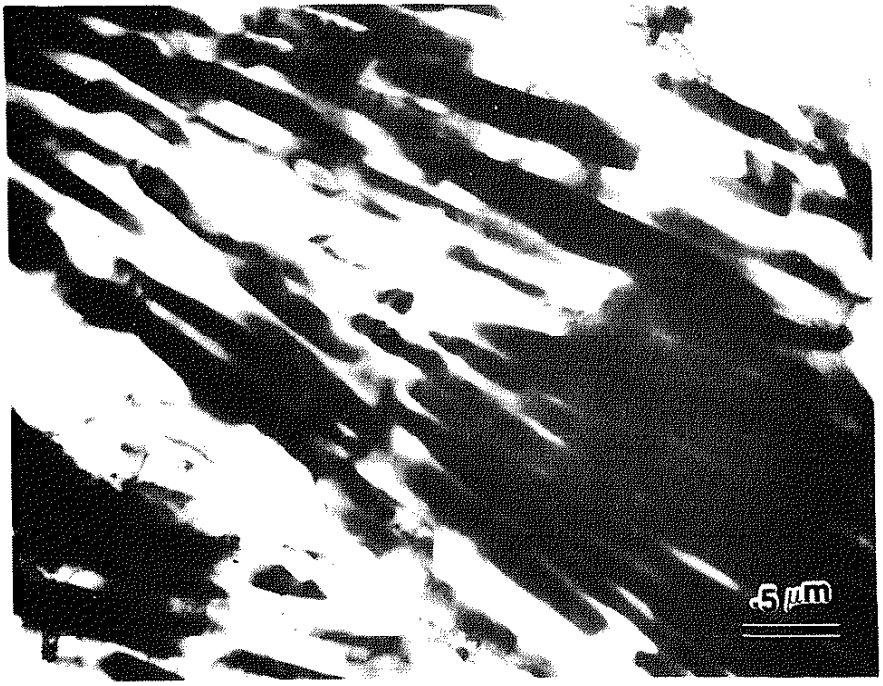

Figure 11(a) Electron Micrograph of the laser clad region showing the elongated M_7C_3 Type (hcp) carbide precipitate

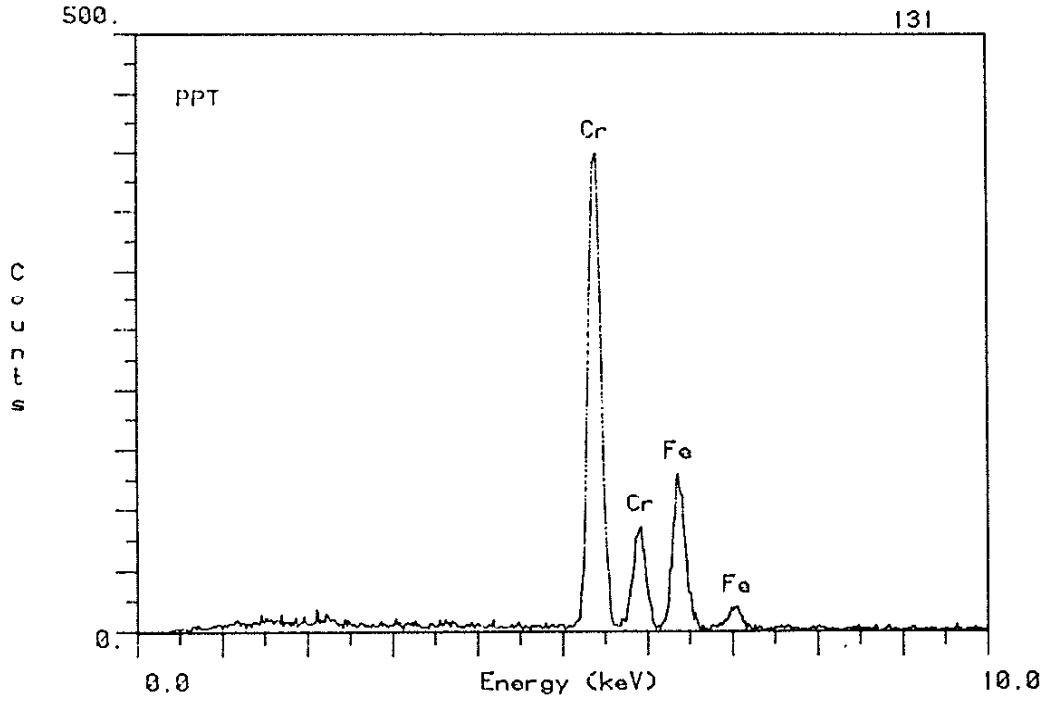

Figure 11(b) The STEM X-Ray micro analysis of the M_7C_3 Type Carbide Precipitate

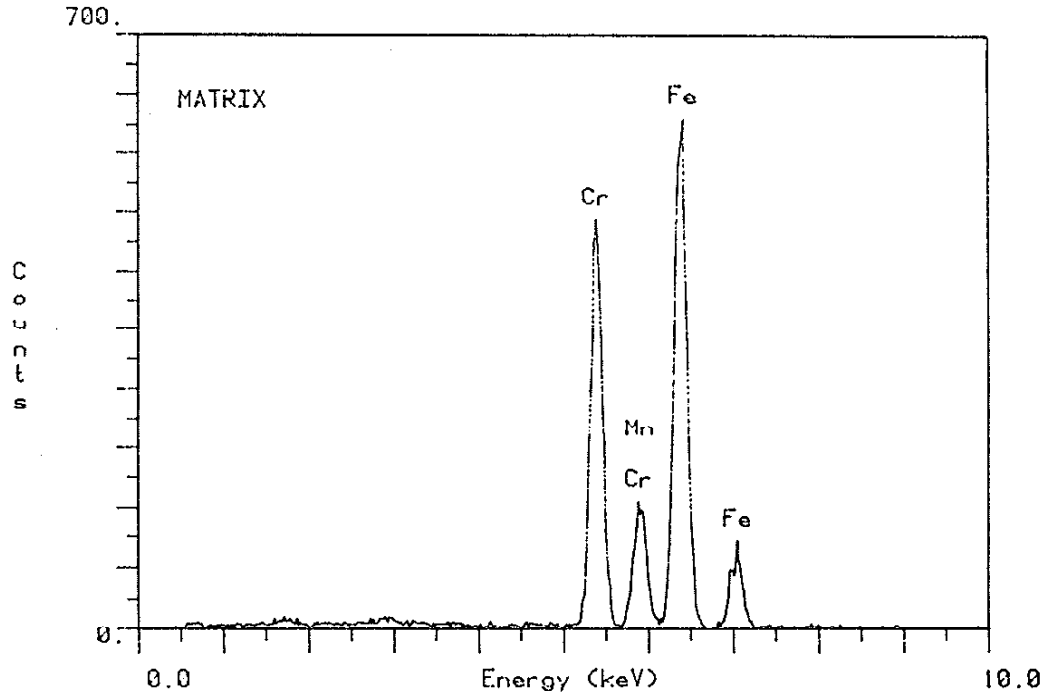

Figure 12 The STEM x-ray microanalysis of the matrix showing equal contents of Fe and Cr

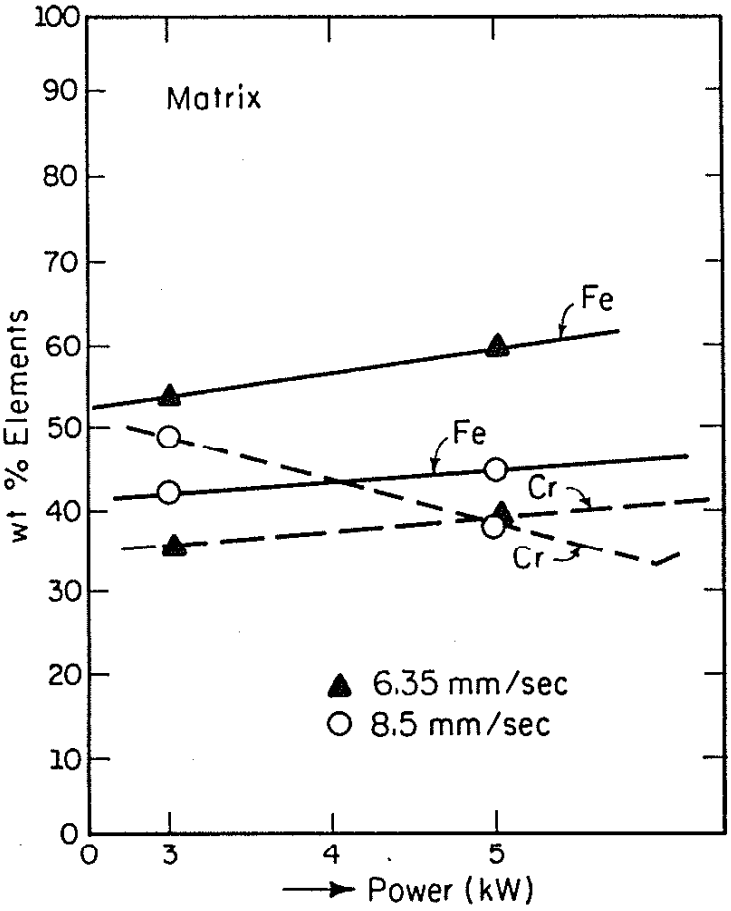

Figure 13 Plot of wt% alloying elements versus laser power (Kw) at different traverse speed.